PROCEEDINGS OF SCIENCE

The effects of high energy radiation on exoplanets, from atmosphere evaporation to habitability

Riccardo Spinelli[a,*]

[a] *INAF – Osservatorio Astronomico di Palermo, Piazza del Parlamento 1, 90134 Palermo (PA), Italy*

E-mail: riccardo.spinelli@inaf.it

At the time of writing, more than 5900 exoplanets have been identified, and thousands more await confirmation. It is now believed that, on average, every star in our Galaxy hosts at least one planet in orbit around it. A non-negligible fraction of these trillion worlds may be Earth-like. Among the main goals of exoplanet research are identifying the key formation and evolution processes that shape the observed demographics (e.g., radius and mass distributions), understanding the range of suitable conditions for life, and, ultimately, pinpointing reliable observational biosignatures for current and next generation IR/optical facilities. In this context, high-energy radiation from the host star and, less frequently, from galactic transient events plays a crucial role, resulting important in assessing the likelihood of planetary atmospheric retention and, therefore, in identifying targets that are suitable for life. This study resumes some results obtained about the process of hydrodynamic atmospheric escape and the twofold (constructive and destructive) effects of high-energy radiation on the emergence and maintenance of life.

Frontier Research in Astrophysics – IV (FRAPWS2024)
9-14 September 2024
Mondello, Palermo, Italy

*Speaker

https://pos.sissa.it/

PoS(FRAPWS2024)062

Introduction

Since the initial detection of exoplanets around a solar-type star [1], the count of confirmed exoplanets has risen exponentially. As of today, over 5900 exoplanets have been identified, with thousands more awaiting further confirmation.

From this expanding sample, some broad conclusions are emerging. The data suggest that i) exoplanets are ubiquitous: statistically, each star in the Milky Way likely hosts at least one exoplanet; ii) planets exist in the universe that have no equivalent in our solar system (such as hot Jupiters and super-Earths); iii) many discovered exoplanets orbit their stars at distances smaller than Mercury's orbit. These proximity conditions expose them to stronger radiation fields, with major consequences for both their atmospheric evolution and potential habitability.

The field of exoplanet research is now shifting from an epoch of discovery to an epoch of characterization, with two core objectives: understanding planetary demographics and identifying planets with life-supporting conditions. In both areas, high-energy radiation (from the host star or, less commonly, from galactic transient events) is central. This radiation spans ultraviolet to X-ray and γ-ray wavelengths, and can break molecules apart, ionize gases, and chemically alter or even strip planetary atmospheres.

High energy radiation can be classified into X-rays and extreme ultraviolet (XUV, 0.5-90 nm), near-ultraviolet (NUV, 200–280 nm), and gamma rays (keV–MeV). These forms of radiation originate from different stellar mechanisms and evolution stages and have varying effects on atmospheric chemistry and habitability.

Section 1 addresses the process of atmospheric hydrodynamic escape under XUV exposure. Section 2 explores how NUV radiation may influence the origin and the presence of life. Section 3 evaluates the potential role of gamma rays from energetic transients in affecting planetary habitability on galactic scales.

1. XUV radiation: evaporating atmospheres

Although EUV (10–90 nm) and X-ray (0.5–10 nm) radiation, collectively termed XUV, represent only a minor portion of stellar output, they can intensely heat planetary upper atmospheres and induce hydrodynamic escape or photoevaporation [e.g., 3–6]. Due to their respective photon energies, EUV is absorbed in the upper atmospheric layers, while X-rays penetrate more deeply.

Photoevaporative loss has been detected in several close-in exoplanets. A remarkable case is GJ 436b [7], a Neptune-like planet with a 2.6-day orbit around a 0.45 solar mass star. It absorbs $\sim$1.35 W/m^2 of XUV flux and loses about six thousand tons of atmosphere per second [8], forming a massive hydrogen tail [9–11].

For exoplanets near their stars, XUV energy input can rival their atmospheric binding energy. This can lead to substantial atmospheric erosion, affecting long-term mass distribution [12, 13]. Photoevaporation is thought to explain observed gaps in the exoplanet radius-period and mass-period distributions [14]. These include the radius valley [15–17], a paucity of planets near $2R_\oplus$, and the Neptunian desert [18–21], a lack of $\sim$0.1 M_J planets with very short orbits.

Photoevaporation is driven by atomic photo-ionization. For example, an XUV photon ionizes hydrogen, liberating an electron with kinetic energy. Some of this energy heats the surrounding gas, leading to expansion and escape (adiabatic cooling), while the rest is lost with other radiative processes such as bremsstrahlung, recombination, collisional excitation, and ionization (radiative cooling). These cooling processes increase with atmospheric temperature [22–24]. The competition between adiabatic and radiative cooling determines the net mass-loss rate.

Historically, the first analytical formulation to estimate the atmospheric mass loss driven by XUV radiation was proposed by Watson et al. [25]. If we define R_{XUV} as the altitude where the bulk of the stellar XUV flux is absorbed (i.e., where the optical depth reaches unity), the total incoming power from XUV radiation is the stellar XUV flux at the orbital separation, F_{XUV}, multiplied by the surface area πR^2_{XUV}. Assuming full conversion of this energy into mechanical expansion, energy conservation yields the equation: $GM_P\dot{M}/R_P = \pi R^2_{XUV}F_{XUV}$, where G is the gravitational constant, $\dot{M}$ is the atmospheric escape rate, and M_p and R_p are the planetary mass and radius. This is known as the *energy-limited* escape formula, used to estimate the upper limit on mass loss due to XUV exposure. Over time, this equation has been refined to include various physical corrections [e.g., 26, 27]. For instance, a factor η (evaporation efficiency), generally in the range 0.3–1, was added to account for two poorly constrained aspects: (1) the portion of incoming XUV energy lost via radiative cooling rather than powering escape, and (2) the uncertain value of $R_{\rm XUV}$, often approximated as a multiple of the planetary radius. Consequently, the most widely used form of the energy-limited approximation for atmospheric escape is:

$$\dot{M} = \eta\frac{3F_{\rm XUV}}{4GK\rho_p}, \tag{1}$$

where G is the gravitational constant, ρ_p is the planet's average density, and K (less than 1) accounts for gravitational effects from the host star [26]. To first order, the atmospheric escape rate $\dot{M}$ is directly proportional to the stellar XUV flux and inversely proportional to the planet's density.

Over the past twenty years, multiple research teams [e.g., 4–6, 28, 29, 31–33, 42] have developed advanced models of atmospheric escape that include additional physical effects such as stellar wind interactions. These models aim to better constrain parameters like $R_{\rm XUV}$ and the proportion of XUV radiation lost through radiative cooling. In particular, several hydrodynamic simulation codes have been created to model photoevaporating atmospheres of exoplanets. These tools incorporate various levels of approximation in radiative transfer, thermodynamic processes, and chemical reactions.

Multi-dimensional hydrodynamical simulations, especially in two and three dimensions [34, 35, e.g.,], target specific exoplanets with high levels of physical and chemical detail. Such simulations have been applied to planets including GJ 436 b [10, 36], HD 209458 b [37–40], and HD 189733 b [41]. These models can reproduce observed features from transit spectroscopy campaigns with remarkable precision, but they require substantial computational resources and are not frequently made publicly accessible.

To mitigate these limitations, one-dimensional hydrodynamic models [42–45] provide a more tractable alternative, capable of delivering realistic escape rates with far lower computational costs. This efficiency enables simulations across a broad range of planetary parameters, such as varying gravitational binding energies and incident XUV fluxes, and aids in identifying optimal candidates for spectroscopic observations. Assuming spherical symmetry, these models generally solve the one-dimensional Euler equations, along with mass and energy conservation, to describe atmospheric gas dynamics under the influence of planetary gravity, while simultaneously incorporating radiative transfer calculations.

A publicly accessible and computationally efficient 1-D hydrodynamic code is ATmospheric EScape[1] [ATES, 45]. ATES is a one-dimensional hydrodynamic solver coupled to a photoionization equilibrium module that accounts for cooling through bremsstrahlung, recombination, and collisional excitation and ionization. It computes the thermodynamic structure (temperature, density, velocity, and ionization fraction) of highly irradiated, primordial exoplanetary atmospheres composed of atomic hydrogen and helium. While overcoming some limitations of the energy-limited approximation, ATES still provides escape rates in close agreement with those produced by more sophisticated hydrodynamical tools (e.g., PLUTO-CLOUDY Interface), but with drastically reduced computational time (typically ranging from a few minutes to several hours on a standard laptop).

Using ATES, Caldiroli et al. [24] carried out extensive simulations to examine the conditions under which the energy-limited prescription overestimates mass loss (i.e., when the efficiency parameter η in Eq. 1 drops well below unity). Results from these simulations are presented in Fig. 1, which plots the effective efficiency $\eta_{\rm eff}$ (defined as the ratio between ATES-estimated outflow rates and those predicted by the energy-limited model with $\eta = 1$) against the specific planetary gravitational potential $\phi_p = GM_p/R_p$, taken as a positive quantity. A total of 16 planets were modeled, and for 8 of them, Caldiroli et al. [24] ran 81 simulations covering a broader range of XUV flux values $F_{\rm XUV}$. Colored points in Fig. 1 indicate different levels of stellar irradiation (in erg cm^{-2} s^{-1}). The figure highlights the existence of a threshold potential $\phi_p^{\rm thr}$, beyond which unity efficiency is unattainable. This threshold can be analytically derived by comparing ion binding energy with the volume-averaged mean excess energy per ion [24]. For $\log \phi_p \geq \log \phi_p^{\rm thr} \sim [12.9\text{–}13.2]$ in cgs units, atmospheric escape is suppressed since most of the absorbed energy is dissipated through local radiative processes due to inefficient energy transfer from photo-electrons to atmospheric ions, reducing η by up to four orders of magnitude (see Fig. 1).

In contrast, whether low-gravity planets ($\phi_p \leq \phi_p^{\rm thr}$) exhibit near-unity efficiency primarily depends on the stellar flux. For $F_{\rm XUV} \lesssim 10^{4-5}$ erg cm^{-2} s^{-1}, adiabatic expansion dominates the cooling budget. These atmospheres are loosely bound, and energy deposition occurs at altitudes where photo-electron collisions impart sufficient kinetic energy to allow atmospheric escape. When $F_{\rm XUV} \gtrsim 10^{4-5}$ erg cm^{-2} s^{-1}, temperatures rise, and radiative plus advective cooling surpass adiabatic expansion, causing η to drop. For high-gravity planets, cooling becomes saturated even at lower fluxes; in such cases, η increases with $F_{\rm XUV}$ but remains well below one. In summary, Caldiroli et al. [24] showed that the energy-limited framework yields realistic results (with $\eta_{\rm eff}$ ranging between 0.3 and 1) only for low-gravity planets under moderate irradiation levels ($F_{\rm XUV} \lesssim 10^{4-5}$ erg cm^{-2} s^{-1}).

The speed and flexibility of the `ATES` code have enabled a variety of applications in the study of atmospheric mass loss from exoplanets. Specifically, it has been employed to: (1) estimate mass-loss rates for a sample of nearby exoplanets orbiting stars with detected X-ray emission [8]; (2) construct a self-consistent modeling pipeline for interpreting He I triplet transit observations [46], yielding simultaneous predictions for He I absorption, thermodynamic outflow structures, and

[1] The code can be accessed at https://github.com/AndreaCaldiroli/ATES-Code

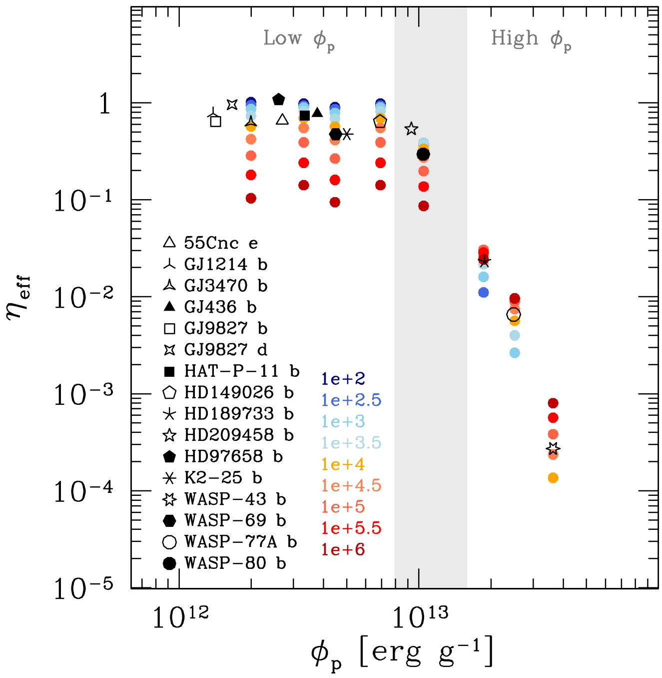

Figure 1: Effective outflow efficiency η_{eff} vs. planetary gravitational potential ϕ_p for 16 exoplanets. η_{eff} is the ratio between the mass loss rate from ATES and the energy-limited formula assuming $\eta = 1$. 81 simulations were run on 8 planets over a broad range of F_{XUV} values. Colors encode F_{XUV}, from 10^2 erg cm^{-2} s^{-1} (dark blue) to 10^6 erg cm^{-2} s^{-1} (dark red), spaced at 0.5 dex intervals. Adapted from Caldiroli et al. [24].

escape rates; (3) interpret observed He I and Hα signatures in systems such as TOI-5398 b [47] and GJ 3470 b [48]; (4) explore the potential for atmospheric escape in hypothetical planets orbiting white dwarfs [49]; and (5) reconstruct the evolutionary history and forecast the future atmospheric loss of photoevaporating planets, including TOI-5398 b [50] and TOI-1430 b [51].

2. Near-ultraviolet radiation: a trigger for the origin of life?

Recent progress in exoplanet demographics is shedding light on the prevalence of Earth-like worlds, particularly their occurrence around low-mass stars. Population synthesis studies [e.g., 52–55] indicate that most M-dwarfs (0.1–0.8 M$_\odot$), which comprise roughly 75% of the stellar population in the Galaxy [56], host at least one small rocky planet (0.5–2.0 R$_\oplus$).

On the theoretical side, a central question is whether such planets can support life as we know it. Since liquid water is crucial for life on Earth, a planet is considered potentially habitable if it lies within the Circumstellar Habitable Zone (CHZ), the region around a star where temperatures allow surface water to remain in a liquid state [e.g., 57, 58]. The extent of the CHZ depends primarily on stellar properties (e.g., luminosity and T_{eff}) and the orbital distance but is also influenced by factors like planetary mass [59], tidal locking [60, 61], atmospheric composition [63–65], and volcanic activity [66]. Tectonics and internal geophysical activity may further shape surface conditions, possibly enhancing habitability [see 67].

Another critical factor is the high-energy radiation environment, shaped by the host star or occasionally by rare transient astrophysical events [e.g., 68–73] (see also Section 3 and [74] for a review). UV and X-ray radiation may negatively affect habitability by driving atmospheric mass loss [8, 75, 76] and degrading biomolecules [77, 78]. However, laboratory experiments [e.g., 79–84] suggest that NUV photons are also essential for prebiotic chemistry, facilitating the synthesis of fundamental biomolecular precursors like RNA.

Spinelli et al. [85] and Spinelli et al. [86] (S23 hereafter) explored the dual role of stellar UV radiation (both destructive and constructive) on potentially habitable planets and proposed the Ultraviolet Habitable Zone (UHZ). This zone is defined as the orbital region around a star where NUV radiation is sufficient to drive prebiotic chemistry but not so intense as to destroy biomolecules or strip atmospheres. Using archival observations from the Ultra-Violet Optical Telescope [UVOT; 87] aboard the *Neil Gehrels Swift Observatory* [70], Spinelli et al. [86] studied 23 planets within the CHZ of 17 M-dwarf stars, suggesting that the current near-ultraviolet (NUV) luminosity of these old M-dwarfs (ages >2.4 Gyr) is too low to sustain abiogenesis driven by cyanosulfidic chemistry [84], casting doubt on the possibility of abiogenesis under present conditions.

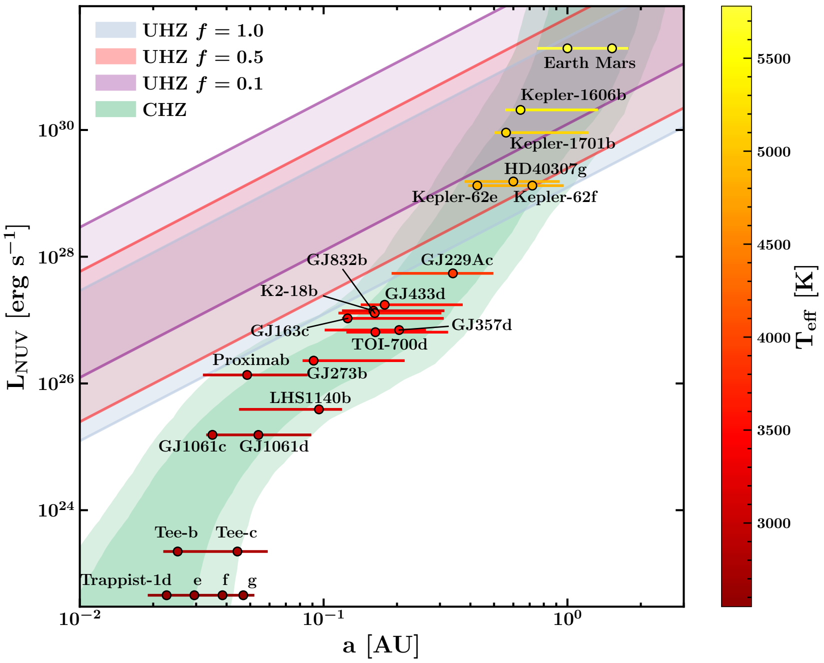

Figure 2: NUV (Near Ultra-Violet) luminosity versus star–planet separation. The UHZ is bounded by flux thresholds for the persistence of prebiotic chemistry and biomolecule stability. We show UHZs for three different surface transmission factors f = 0.1, 0.5, and 1.0. The CHZ planets from our sample are shown as circles, color-coded by their host stars' effective temperature. Horizontal bars denote the CHZ of each system as computed by [58], while green shaded bands indicate the CHZ. Adapted from S23.

However, given that these stars were likely more UV-luminous during their youth, S23 hypothesized that CHZ planets might have received sufficient NUV radiation early in their evolution to enable the onset of life. This hypothesis is tested in Spinelli et al. [88] (S24 hereafter), where GALEX-based UV luminosity measurements of young stellar associations [89, hereafter R23] are used to reconstruct the temporal evolution of both the CHZ and UHZ for the stars analyzed in S23. This allows to assess whether and when an overlap between the two zones may have occurred in the past.

S24 selected a stellar sample from S23 composed of 14 planetary systems hosting rocky planets within the conservative habitable zone (CHZ), observed in the near-ultraviolet (NUV) by Swift, and having reliable age estimates and stellar masses below 0.9 $M_\odot$. The CHZ limits are adopted optimistically as in S23, based on empirical evidence of past liquid water presence on Mars and Venus [57, 58]. To model the temporal evolution of the CHZ, S24 employed MESA Isochrones and Stellar Tracks [MIST 90, 91] providing stellar parameters over time, allowing the calculation of the inner and outer CHZ boundaries following [59].

For the ultraviolet habitable zone (UHZ), S24 used the NUV evolution results from R23 derived from GALEX observations of M and K stars in young moving groups and the field, spanning ages from 10 Myr to 5 Gyr. NUV fluxes were rescaled to match the 200–280 nm band relevant to Rimmer et al. [84] by converting GALEX and Swift flux densities and assuming flat NUV spectra within this range. Figure 3 illustrates the NUV luminosity evolution with stellar age for different spectral subtypes. Each star's NUV evolution was normalized to its current Swift-measured luminosity, accounting for age uncertainties by considering evolutionary tracks at estimated, upper, and lower age limits, enabling time-dependent boundaries of the UHZ to be derived.

Figure 4 illustrates the temporal evolution of the CHZ (green shaded area) and UHZ (shaded in violet, red, and grey) for each host star in the seleced sample, where the UHZ is calculated assuming three atmospheric NUV transmittance values: 10%, 50%, and 100%. These values represent atmospheres with increasing transparency to NUV radiation, related to different concentrations of atmospheric absorbers such as CO_2. The vertical gray lines indicate literature estimates of stellar ages. The bottom panels show the fraction of overlap between CHZ and UHZ over time, reflecting periods when planetary surfaces receive NUV flux compatible with habitability criteria under varying atmospheric conditions.

Figure 5 quantifies, as a function of host effective temperature, the total duration during which the radial overlap between CHZ and UHZ exceeds 25%, for each atmospheric transmission scenario. Data points include uncertainties derived from the assumed age ranges or lower limits. Notably, some systems lack overlap at certain transmittance levels, indicating limited temporal windows for simultaneous liquid water and sufficient NUV flux. These results highlight the critical interplay between stellar evolution, atmospheric properties, and potential planetary habitability.

The analysis of S24 confirms and extends previous findings (S23) that, in cool stars ($T_{\rm eff}$ <3900 K) such as Trappist-1, GJ 273, Proxima Centauri, K2-18, GJ 832, and GJ 357, the present-day CHZ and the UHZ do not currently overlap (see Fig. 4). A marginal overlap is observed in GJ 229A for 100% NUV atmospheric transmission, while for K-type stars (Kepler-62 and HD 40307) the CHZ is almost entirely encompassed by the UHZ, assuming both 100% and 50% NUV transparency. This implies that planets in their CHZs may receive sufficient NUV radiation to enable prebiotic chemistry, as described by Rimmer et al. [84]. CHZ-UHZ overlaps were more substantial, especially around hotter stars. For most systems, an intersection was present within the first 1–2 Gyr of evolution, except for the coolest M-dwarfs ($T_{\rm eff} \lesssim$ 2800 K). Stars with $T_{\rm eff} \gtrsim$ 3500 K, such as GJ

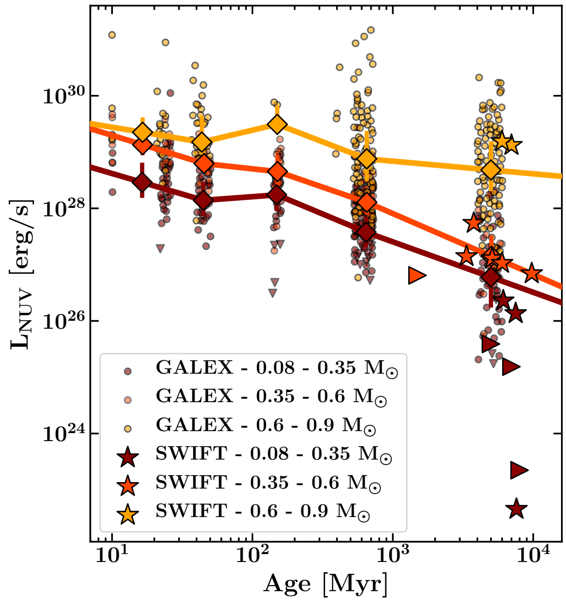

Figure 3: Dots (downward triangles) represent NUV luminosities estimated using GALEX data (upper limits) as reported in R23 for late-M-dwarfs (red), early-M-dwarfs (orange) and K stars (yellow). Diamond symbols represent the median NUV luminosity values at each age bin (same color coding) and solid lines are piece-wise linear interpolations among consecutive time bins. Star symbols represent the NUV luminosities of the selected sample stars, as measured from Swift/UVOT observations, at the time corresponding to the age of these stars reported in the literature. The same color coding highlights late-M-dwarfs (red), early-M-dwarfs (orange) and K stars (yellow). Stars with only a lower limit estimate of their age are shown with red and orange rightward triangles. Adapted from S24.

229A, GJ 357, Kepler-62, and HD 40307b, exhibited extended past overlaps even under conservative (10%) NUV transmission assumptions.

In intermediate-temperature M-dwarfs ($T_{eff} \lesssim 3400$ K), overlaps exceeding 25% of CHZ radial extent lasted up to ~700 Myr (grey UHZ) and ~300 Myr (red UHZ). An outlier is Proxima Centauri, with ~3.3 Gyr (~1.5/0.12 Gyr) overlap with grey (red/violet) UHZ. Even assuming an older age estimate (4.8 Gyr; [62]), significant overlap persists.

For stars with $3500\,\mathrm{K} \lesssim T_{eff} \lesssim 4000\,\mathrm{K}$, more than 25% overlap occurred even under 10% transmission scenarios. For example, in GJ 357, such overlap persisted for ~3.0/1.6/0.3 Gyr (grey/red/violet). In K-type stars, this overlap decreases after ~500 Myr, but persists (grey/red UHZ) to present and into the post-main-sequence phase.

Average durations of >25% CHZ-UHZ overlap vary by spectral type and NUV transmission: - Late M-dwarfs (T_{eff} 2800–3400 K): ~1.3/0.5/0.03 Gyr (100/50/10% transmission) - Early M-dwarfs (T_{eff} 3400–3900 K): ~2.2/1.2/0.2 Gyr - K-type stars: ~28/20/0.5 Gyr

These estimates neglect atmospheric evolution, which could significantly alter NUV transparency over time. Fig. 4 also shows the age at which rocky planets are likely to lose their primordial envelopes, based on NGPPS simulations [92]. Yellow/orange lines denote times when 20–40% of systems host envelope-free rocky planets in the CHZ.

While prior works [84, 93] argued that M-dwarfs are generally too faint in the NUV to

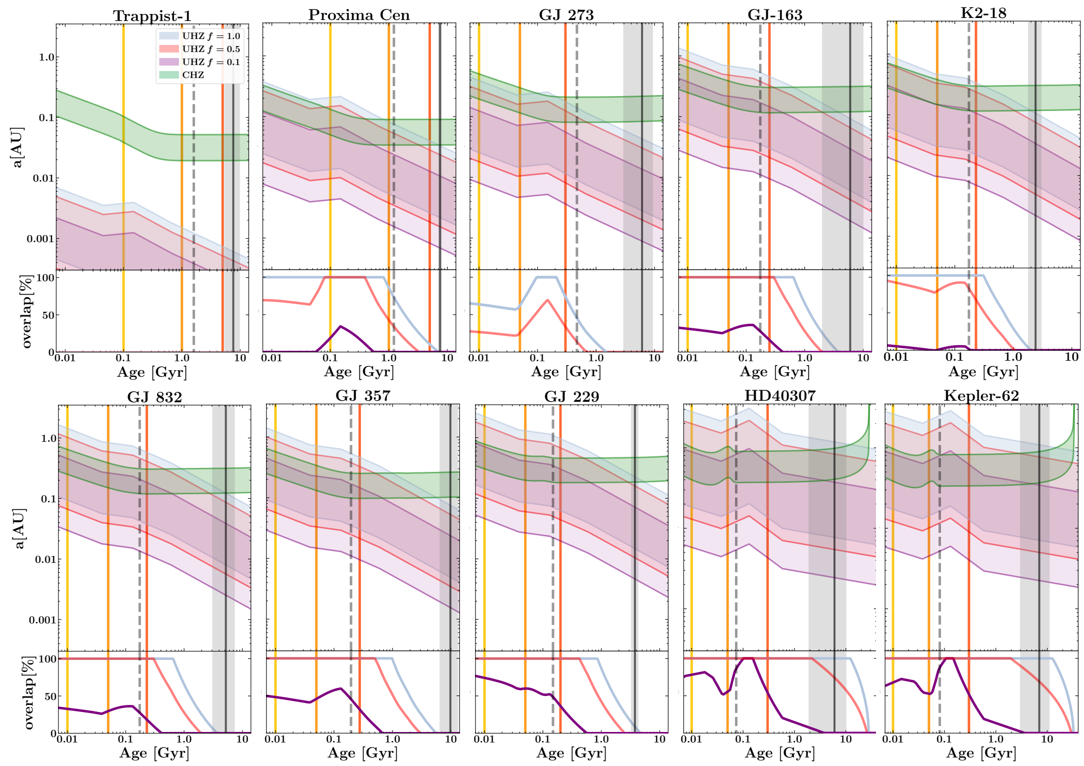

Figure 4: Top panels: evolution of CHZ and UVH for Trappist-1, Proxima Centauri, GJ 273, GJ 163, K2-18, GJ 832, GJ 357, GJ 229A, HD 40307 and Kepler-62. In each plot the vertical gray line represents the host star age found in the literature and the relative errors (the gray shaded region around the gray line). Yellow, orange and dark orange lines represent the ages at which fraction of systems with at least one rocky planet without a primordial envelope in the CHZ is equal to 20%, 30%, 40% for each system (according to NGPPS model). The dashed line represents the time where each star settled onto the main sequence. Bottom panels: evolution of the fraction of the radial extension of the CHZ that is overlapping the radial extension of the UVZ for three different values of the NUV atmospheric transmission. Adapted from S24.

support abiogenesis via cyanosulfidic pathways, the results obtained by S24 challenge this view. By considering NUV luminosity evolution, S24 find that many M-dwarfs emitted sufficient NUV flux during their early evolution to support prebiotic chemistry. The main exceptions are the coldest M-dwarfs ($T_{\rm eff} \lesssim 2800$ K), such as Trappist-1 and Teegarden's Star.

3. The impact of gamma-ray radiation: high energy transients and extinction events

Gamma-ray radiation is not produced during the stable burning phases of stellar evolution (i.e., the main sequence), but rather during the final stages of massive stars. Gamma-ray bursts (GRBs), for example, are intense flashes of high-energy radiation emitted during the collapse of rapidly rotating massive stars or the merger of two neutron stars (e.g. see Kumar & Zhang [94] for a recent review). Supernovae (SNe), instead, result from the explosion of either massive stars or white dwarfs in binary systems. The energies involved in these events are extreme: a GRB can emit in 10 seconds the same amount of energy that an entire galaxy like the Milky Way (with over 100 billion stars) emits in 100 years.

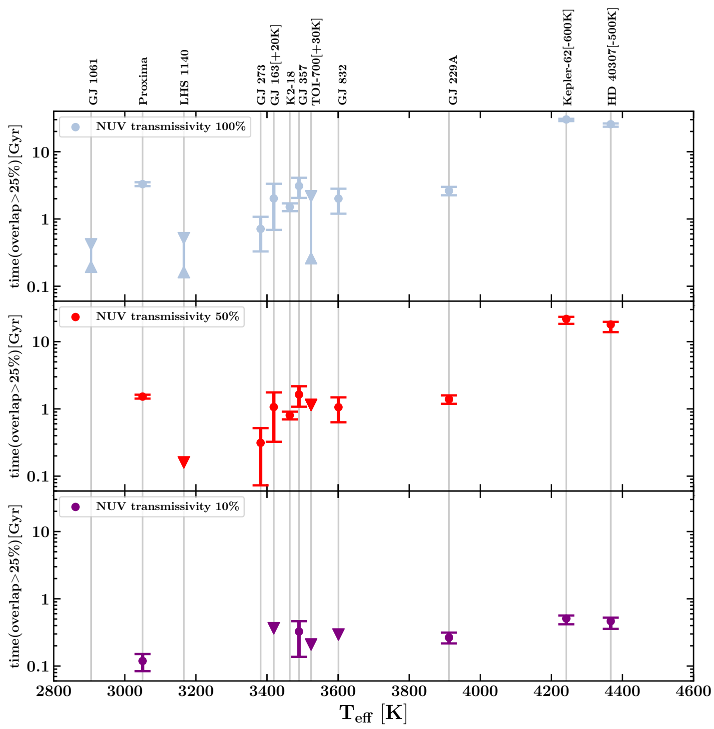

Figure 5: Time during which for each host star there is a fractional overlap greater than 25% (violet, red, grey dots) between the radial extension of CHZ and UVH for the three different atmospheric NUV transmission (10%, 50%, 100% respectively). Triangle symbols represent the upper and lower limits. Adapted from S24.

In addition to the main and local factors that may influence the presence and the emergence of life as we know it, several studies suggest that planetary habitability can also be influenced by the radiation produced on the larger scales (from parsec to kiloparsec) within the Galaxy [68–72]. Indeed, intense high energy radiation fluxes, also over relatively short timescales, can produce major changes on the planetary atmosphere and/or result directly lethal for the biota.

A typical GRB for example, emitting an isotropic equivalent energy $\sim 10^{52}$ erg s^{-1}, can illuminate a planet at one kiloparsec distance with a γ-ray (i.e., keV–MeV) fluence $\sim$100 kJ m^{-2}. This is able, for example, to destroy most of the ozone layer of an Earth like atmospheres [95] and thus expose the biota to harmful UVB radiation from the parent star. In this case, intense UVB radiation could also be lethal to surface marine life such as phytoplankton, which is fundamental for the food chain and oxygen production. Moreover, the opacity of the NO_2 produced in the stratosphere would reduce the visible sunlight that reaches the surface, causing a global cooling. Melott et al. [96] proposed that the late Ordovician ME event ($\sim$ 445 Myr ago), which is one of the five great mass extinctions on Earth, was triggered by a GRB.

The natural extension of these works focused on Earth were aimed at studying the Galaxy as a whole, thus constraining the regions and cosmic epochs where life may have been less subject to threatening astrophysical high energy transients [97–105]. Stellar evolution models show that SNe preferentially occur in star-forming regions where massive stars are born [106–108]. GRBs, instead, are favored in star-forming environments with low metallicity, where massive stars experience weaker stellar winds and thus retain rapid rotation, a condition necessary to launch a GRB during core collapse [109–114]. For this reasons, understanding where these catastrophic events occur within the Galaxy requires galactic evolution models (i.e. the evolution of the star formation rate and the metallicity with in the Galaxy). Generally, these models predict that the inner regions of the Milky Way formed quickly in its early history, about 10 billion years ago, while star formation gradually increased in the outer regions [115]. As a result, the interstellar medium in the inner Galaxy became metal-rich early on, while the outskirts enriched more slowly and never reached the same metallicity levels.

Based on this framework, Spinelli et al. [73] estimated the spatial and temporal distribution of astrophysical transients capable of inducing biospheric damage within the Milky Way. They rescaled the cosmological event rate of transients capable of depleting the ozone layer (such as GRBs and SNe) within the Milky Way, taking into account both the observational constraints on these events (e.g., their preference for low-metallicity and high star-forming environments) and the internal evolution of the Galaxy in terms of metallicity and star formation rate [116].

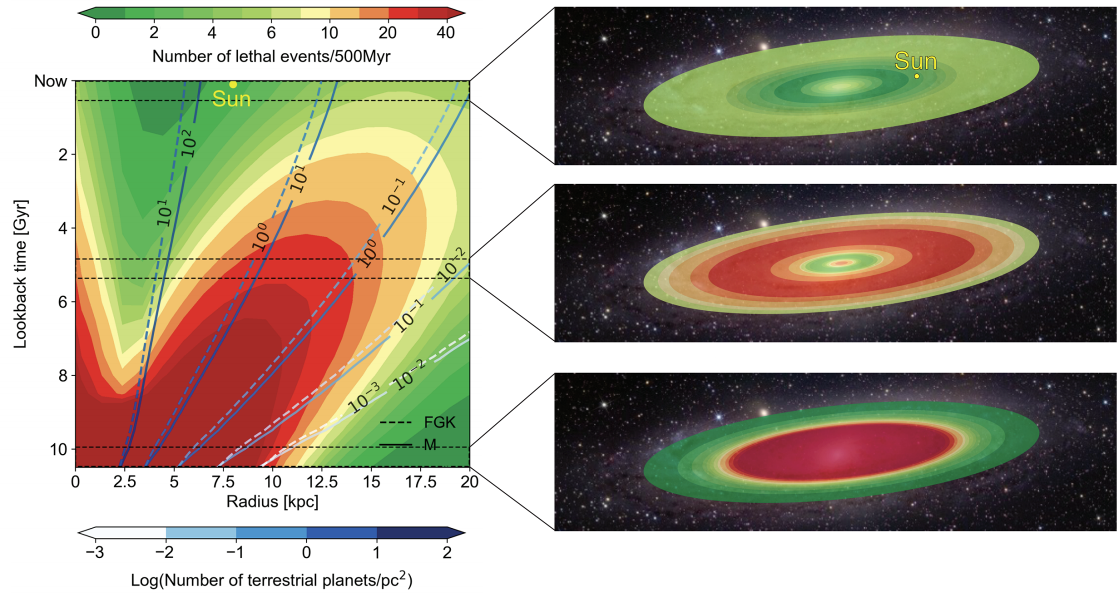

Figure 6: Number of lethal events (combining GRBs – long and short – and SNe) as a function of the galactocentrinc radius and lookback time (left panel). The shaded contours (referred to the color bar on top of the plot) show the number of lethal events per bins of 0.5 Gyrs. The line contours (corresponding to the color bar at the bottom of the plot) show the surface number density of terrestrual planets around M stars (solid lines) and FGK stars (dashed lines). The current position of the Solar System is marked by the yellow dot. The three right panels are artistic representation of the Galaxy habitability in three representative epochs with a similar color cording of the upper bar (i.e. representing the number of lethal events).

Assuming that the transient sources follow the stellar distribution, the number of potentially lethal events per unit redshift z for a planet located at galactocentric radius R is given by:

$$\frac{dN_{MW}(R,z)}{dz} = \frac{V_{MW}(z)}{M_\star(z)} \int_L \int_{S_H(L)} \xi(L,z)\Sigma_\star(s,R,z) f_{Fe}(s,R,z) f_{sSFR}(s,R,z) dL\, ds \quad (2)$$

Here, $\xi(L, z)$ is the luminosity function of the source class, $S_H(L)$ the hazard area associated with a given luminosity L, and $\Sigma_\star(s, R, z)$ the stellar surface density within the hazard area (the area within which a transient even hit a planet with a fluence greater than 100 J m^{-2}). V_{MW} is cosmological volume occupied by our Galaxy while $M_\star$ is its stellar mass. The dimensionless factors $f_{Fe}(s, R, z)$ and $f_{sSFR}(s, R, z)$ account for the local metallicity and specific star formation rate relative to cosmic averages, respectively. This formalism allows a spatially resolved, time-dependent estimate of transient rates relevant for planetary habitability [for details see 74].

The results obtained by Spinelli et al. [73] indicate that until around 6 billion years ago, planets (except in the outermost regions which are poor in planets) were exposed to numerous extinction events triggered by high energy transients due to high star formation and low metallicity (Fig. 6). Over time, increasing metallicity suppressed GRB formation in the inner Galaxy (between 2 and 8 kpc from the center), while rising star formation in the outer regions enhanced it.

Except for the very central region (<2 kpc), where SNe dominate, the study suggests that GRBs have been the main evolutionary pressure throughout most of the Galaxy's history. Despite being rarer than SNe, GRBs can affect planets from much greater distances due to their higher energy.

Focusing on the more recent past, the study shows that over the last 500 million years, the Milky Way has been relatively safer. Peripheral regions have remained vulnerable to GRBs, while central ones have been more exposed to SNe. The safest zone during this period is estimated to lie between 2 and 8 kpc from the Galactic center, also the region hosting the highest number of terrestrial planets. At the solar system's distance from the center (8 kpc), Spinelli et al. [73] estimate that one catastrophic GRB occurred in the last 500 million years, consistent with the hypothesis that the Late Ordovician extinction may have been triggered by such an event.

Acknowledgments

The author acknowledges the support of the ARIEL ASI/INAF agreement no. 2021-5-HH.0 and the support of grant no. 2022J7ZFRA – Exo-planetary Cloudy Atmospheres and Stellar High energy (Exo-CASH) funded by MUR – PRIN 2022.

References

[1] Mayor, M. & Queloz, D. A Jupiter-mass companion to a solar-type star. *Nature*. **378**, 355-359 (1995,11)

[2] Borucki, W. J., Koch, D. G., Dunham, E. W., et al. 1997, Planets Beyond the Solar System and the Next Generation of Space Missions, 119, 153

[3] Lammer, H., Selsis, F., Ribas, I., Guinan, E., Bauer, S. & Weiss, W. Atmospheric Loss of Exoplanets Resulting from Stellar X-Ray and Extreme-Ultraviolet Heating. *ApJ*. **598**, L121-L124 (2003,12)

[4] Yelle, R. Aeronomy of extra-solar giant planets at small orbital distances. *Icarus*. **170**, 167-179 (2004,7)

[5] Murray-Clay, R., Chiang, E. & Murray, N. ATMOSPHERIC ESCAPE FROM HOT JUPITERS. *ApJ*. **693**, 23-42 (2009,2)

[6] Owen, J. & Jackson, A. Planetary evaporation by UV and X-ray radiation: basic hydrodynamics. *MNRAS*. **425**, 2931-2947 (2012,10)

[7] Butler, R., Vogt, S., Marcy, G., Fischer, D., Wright, J., Henry, G., Laughlin, G. & Lissauer, J. A Neptune-Mass Planet Orbiting the Nearby M Dwarf GJ 436. *ApJ*. **617**, 580-588 (2004,12)

[8] Spinelli, R., Gallo, E., Haardt, F., Caldiroli, A., Biassoni, F., Borsa, F. & Rauscher, E. Planetary Parameters, XUV Environments, and Mass-loss Rates for Nearby Gaseous Planets with X-Ray-detected Host Stars. *AJ*. **165**, e200 (2023,5)

[9] Kulow, J., France, K., Linsky, J. & Loyd, R. Lyα Transit Spectroscopy and the Neutral Hydrogen Tail of the Hot Neptune GJ 436b. *ApJ*. **786**, e132 (2014,5)

[10] Ehrenreich, D., Bourrier, V., Wheatley, P., Lecavelier des Etangs, A., Hébrard, G., Udry, S., Bonfils, X., Delfosse, X., Désert, J., Sing, D. & Vidal-Madjar, A. A giant comet-like cloud of hydrogen escaping the warm Neptune-mass exoplanet GJ 436b. *Nature*. **522**, 459-461 (2015,6)

[11] Bourrier, V., Lecavelier des Etangs, A., Ehrenreich, D., Tanaka, Y. & Vidotto, A. An evaporating planet in the wind: stellar wind interactions with the radiatively braked exosphere of GJ 436 b. *A&A*. **591** pp. eA121 (2016,6)

[12] Penz, T. & Micela, G. X-ray induced mass loss effects on exoplanets orbiting dM stars. *A&A*. **479**, 579-584 (2008,2)

[13] Penz, T., Micela, G. & Lammer, H. Influence of the evolving stellar X-ray luminosity distribution on exoplanetary mass loss. *A&A*. **477**, 309-314 (2008,1)

[14] Modirrousta-Galian, D., Locci, D. & Micela, G. The Bimodal Distribution in Exoplanet Radii: Considering Varying Core Compositions and H_2 Envelope's Sizes. *ApJ*. **891**, e158 (2020,3)

[15] Owen, J. & Wu, Y. Kepler Planets: A Tale of Evaporation. *ApJ*. **775**, e105 (2013,10)

[16] Lopez, E. & Fortney, J. Understanding the Mass-Radius Relation for Sub-neptunes: Radius as a Proxy for Composition. *ApJ*. **792**, e1 (2014,9)

[17] Fulton, B., Petigura, E., Howard, A., Isaacson, H., Marcy, G., Cargile, P., Hebb, L., Weiss, L., Johnson, J., Morton, T., Sinukoff, E., Crossfield, I. & Hirsch, L. The California-Kepler Survey. III. A Gap in the Radius Distribution of Small Planets. *AJ*. **154**, e109 (2017,9)

[18] Szabó, G. & Kiss, L. A Short-period Censor of Sub-Jupiter Mass Exoplanets with Low Density. *ApJ*. **727**, eL44 (2011,2)

[19] Sanchis-Ojeda, R., Rappaport, S., Winn, J., Kotson, M., Levine, A. & El Mellah, I. A Study of the Shortest-period Planets Found with Kepler. *ApJ*. **787**, e47 (2014,5)

[20] Mazeh, T., Holczer, T. & Faigler, S. Dearth of short-period Neptunian exoplanets: A desert in period-mass and period-radius planes. *A&A*. **589** pp. eA75 (2016,5)

[21] Lundkvist, M., Kjeldsen, H., Albrecht, S., Davies, G., Basu, S., Huber, D., Justesen, A., Karoff, C., Silva Aguirre, V., Van Eylen, V., Vang, C., Arentoft, T., Barclay, T., Bedding, T., Campante, T., Chaplin, W., Christensen-Dalsgaard, J., Elsworth, Y., Gilliland, R., Handberg, R., Hekker, S., Kawaler, S., Lund, M., Metcalfe, T., Miglio, A., Rowe, J., Stello, D., Tingley, B. & White, T. Hot super-Earths stripped by their host stars. *Nature Communications*. **7** pp. e11201 (2016,4)

[22] Hui, L. & Gnedin, N. Equation of state of the photoionized intergalactic medium. *MNRAS*. **292**, 27-42 (1997,11)

[23] Glover, S. & Jappsen, A. Star Formation at Very Low Metallicity. I. Chemistry and Cooling at Low Densities. *ApJ*. **666**, 1-19 (2007,9)

[24] Caldiroli, A., Haardt, F., Gallo, E., Spinelli, R., Malsky, I. & Rauscher, E. Irradiation-driven escape of primordial planetary atmospheres. II. Evaporation efficiency of sub-Neptunes through hot Jupiters. *A&A*. **663** pp. eA122 (2022,7)

[25] Watson, A., Donahue, T. & Walker, J. The dynamics of a rapidly escaping atmosphere: Applications to the evolution of Earth and Venus. *Icarus*. **48**, 150 - 166 (1981)

[26] Erkaev, N., Kulikov, Yu. N., Lammer, H., Selsis, F., Langmayr, D., Jaritz, G. F. & Biernat, H. K. Roche lobe effects on the atmospheric loss from "Hot Jupiters". *A&A*. **472**, 329-334 (2007), https://doi.org/10.1051/0004-6361:20066929

[27] Sanz-Forcada, J., Micela, G., Ribas, I., Pollock, A. M. T., Eiroa, C., Velasco, A., Solano, E. & Garcia-Alvarez, D. Estimation of the XUV radiation onto close planets and their evaporation. *A&A*. **532** pp. A6 (2011)

[28] Tian, F., Toon, O., Pavlov, A. & De Sterck, H. Transonic Hydrodynamic Escape of Hydrogen from Extrasolar Planetary Atmospheres. *ApJ*. **621**, 1049-1060 (2005,3)

[29] Garcia Munoz, A. Physical and chemical aeronomy of HD 209458b. *Planet Space Sci*. **55**, 1426-1455 (2007,7)

[30] Salz, M., Schneider, P. C., Czesla, S. & Schmitt, J. H. M. M. Energy-limited escape revised - The transition from strong planetary winds to stable thermospheres. *A&A*. **585** pp. L2

[31] Erkaev, N., Lammer, H., Odert, P., Kislyakova, K., Johnstone, C., Güdel, M. & Khodachenko, M. EUV-driven mass-loss of protoplanetary cores with hydrogen-dominated atmospheres: the influences of ionization and orbital distance. *MNRAS*. **460**, 1300-1309 (2016,8)

[32] McCann, J., Murray-Clay, R., Kratter, K. & Krumholz, M. Morphology of Hydrodynamic Winds: A Study of Planetary Winds in Stellar Environments. *ApJ*. **873**, e89 (2019,3)

[33] Vidotto, A. & Cleary, A. Stellar wind effects on the atmospheres of close-in giants: a possible reduction in escape instead of increased erosion. *MNRAS*. **494**, 2417-2428 (2020,5)

PoS(FRAPWS2024)062

[34] Debrecht, A., Carroll-Nellenback, J., Frank, A., McCann, J., Murray-Clay, R. & Blackman, E. Photoevaporative flows from exoplanet atmospheres: a 3D radiative hydrodynamic parameter study. *MNRAS*. **483**, 1481-1495 (2019,2)

[35] Esquivel, A., Schneiter, M., Villarreal D'Angelo, C., Sgró, M. & Krapp, L. Hydrodynamical interaction of stellar and planetary winds: effects of charge exchange and radiation pressure on the observed Lyα absorption. *MNRAS*. **487**, 5788-5798 (2019,8)

[36] Khodachenko, M., Shaikhislamov, I., Lammer, H., Berezutsky, A., Miroshnichenko, I., Rumenskikh, M., Kislyakova, K. & Dwivedi, N. Global 3D Hydrodynamic Modeling of In-transit Lyα Absorption of GJ 436b. *ApJ*. **885**, e67 (2019,11)

[37] Koskinen, T., Harris, M., Yelle, R. & Lavvas, P. The escape of heavy atoms from the ionosphere of HD209458b. I. A photochemical-dynamical model of the thermosphere. *Icarus*. **226**, 1678-1694 (2013,11)

[38] Khodachenko, M., Shaikhislamov, I., Lammer, H., Kislyakova, K., Fossati, L., Johnstone, C., Arkhypov, O., Berezutsky, A., Miroshnichenko, I. & Posukh, V. Lyα Absorption at Transits of HD 209458b: A Comparative Study of Various Mechanisms Under Different Conditions. *ApJ*. **847**, e126 (2017,10)

[39] Bisikalo, D., Shematovich, V., Cherenkov, A., Fossati, L. & Möstl, C. Atmospheric Mass Loss from Hot Jupiters Irradiated by Stellar Superflares. *ApJ*. **869**, e108 (2018,12)

[40] Debrecht, A., Carroll-Nellenback, J., Frank, A., Blackman, E., Fossati, L., McCann, J. & Murray-Clay, R. Effects of radiation pressure on the evaporative wind of HD 209458b. *MNRAS*. **493**, 1292-1305 (2020,3)

[41] Odert, P., Erkaev, N., Kislyakova, K., Lammer, H., Mezentsev, A., Ivanov, V., Fossati, L., Leitzinger, M., Kubyshkina, D. & Holmström, M. Modeling the Lynsit absorption of the hot Jupiter HD 189733b. *A&A*. **638** pp. A49 (2020)

[42] Salz, M., Schneider, P. C., Czesla, S. & Schmitt, J. H. M. M. Energy-limited escape revised - The transition from strong planetary winds to stable thermospheres. *A&A*. **585** pp. L2

[43] Kubyshkina, D., Fossati, L., Erkaev, N., Johnstone, C., Cubillos, P., Kislyakova, K., Lammer, H., Lendl, M. & Odert, P. Grid of upper atmosphere models for 1-40 M_⊕ planets: application to CoRoT-7 b and HD 219134 b,c. *A&A*. **619** pp. eA151 (2018,11)

[44] Allan, A. & Vidotto, A. Evolution of atmospheric escape in close-in giant planets and their associated Lyα and Hα transit predictions. *MNRAS*. **490**, 3760-3771 (2019,12)

[45] Caldiroli, A., Haardt, F., Gallo, E., et al. 2021, A&A, Irradiation-driven escape of primordial planetary atmospheres. I. The ATES photoionization hydrodynamics code, 655, A30. doi:10.1051/0004-6361/202141497

[46] Biassoni, F., Borsa, F., Haardt, F., et al. 2024, A&A, High-resolution transmission spectroscopy of the hot-Saturn HD 149026b, 691, A283. doi:10.1051/0004-6361/202451750

[47] D'Arpa, M. C., Guilluy, G., Mantovan, G., et al. 2024, A&A, The GAPS programme at TNG: LXIII. Photo-evaporating puzzle: Exploring the enigmatic nature of TOI-5398 b's atmospheric signal, 692, A77. doi:10.1051/0004-6361/202451237

[48] Guilluy, G., D'Arpa, M. C., Bonomo, A. S., et al. 2024, A&A, The GAPS Programme at TNG. LIV. A He I survey of close-in giant planets hosted by M-K dwarf stars with GIANO-B, 686, A83. doi:10.1051/0004-6361/202348997

[49] Gallo, E., Caldiroli, A., Spinelli, R., et al. 2024, ApJ, Evaporation of Close-in Sub-Neptunes by Cooling White Dwarfs, 966, 1, L1. doi:10.3847/2041-8213/ad3ae3

[50] Mantovan, G., Malavolta, L., Locci, D., et al. 2024, A&A, Orbital obliquity of the young planet TOI-5398 b and the evolutionary history of the system, 684, L17. doi:10.1051/0004-6361/202449769

[51] Nardiello, D., Akana Murphy, J. M., Spinelli, R., et al. 2025, A&A, The GAPS Programme at TNG: LXV. Precise density measurement of TOI-1430 b, a young planet with an evaporating atmosphere, 693, A32. doi:10.1051/0004-6361/202452236

[52] Bonfils, X., Delfosse, X., Udry, S., Forveille, T., Mayor, M., Perrier, C., Bouchy, F., Gillon, M., Lovis, C., Pepe, F., Queloz, D., Santos, N., Ségransan, D. & Bertaux, J. The HARPS search for southern extra-solar planets. XXXI. The M-dwarf sample. *A&A*. **549** pp. eA109 (2013,1)

[53] Dressing, C. & Charbonneau, D. The Occurrence Rate of Small Planets around Small Stars. *ApJ*. **767**, e95 (2013,4)

[54] Dressing, C. & Charbonneau, D. The Occurrence of Potentially Habitable Planets Orbiting M Dwarfs Estimated from the Full Kepler Dataset and an Empirical Measurement of the Detection Sensitivity. *ApJ*. **807**, e45 (2015,7)

[55] Tuomi, M., Jones, H., Barnes, J., Anglada-Escudé, G. & Jenkins, J. Bayesian search for low-mass planets around nearby M dwarfs - estimates for occurrence rate based on global detectability statistics. *MNRAS*. **441**, 1545-1569 (2014,6)

[56] Bochanski, J., Hawley, S., Covey, K., West, A., Reid, I., Golimowski, D. & Ivezić, Ž. The Luminosity and Mass Functions of Low-mass Stars in the Galactic Disk. II. The Field. *AJ*. **139**, 2679-2699 (2010,6)

[57] Kasting, J., Whitmire, D. & Reynolds, R. Habitable Zones around Main Sequence Stars. *Icarus*. **101**, 108-128 (1993,1)

[58] Kopparapu, R., Ramirez, R., Kasting, J., Eymet, V., Robinson, T., Mahadevan, S., Terrien, R., Domagal-Goldman, S., Meadows, V. & Deshpande, R. Habitable Zones around Main-sequence Stars: New Estimates. *ApJ*. **765**, e131 (2013,3)

[59] Kopparapu, R., Ramirez, R., SchottelKotte, J., Kasting, J., Domagal-Goldman, S. & Eymet, V. Habitable Zones around Main-sequence Stars: Dependence on Planetary Mass. *ApJ*. **787**, eL29 (2014,6)

[60] Driscoll, P. & Barnes, R. Tidal Heating of Earth-like Exoplanets around M Stars: Thermal, Magnetic, and Orbital Evolutions. *Astrobiology*. **15**, 739-760 (2015,9)

[61] Barnes, R. 2017, Celestial Mechanics and Dynamical Astronomy, 129, 509

[62] Bazot, M., Christensen-Dalsgaard, J., Gizon, L. & Benomar, O. On the uncertain nature of the core of α Cen A. *MNRAS*. **460**, 1254-1269 (2016,8)

[63] Goldblatt, C., Robinson, T. D., Zahnle, K. J., et al. Bistability of Atmospheric Oxygen and the Great Oxidation: Implications for Life Detection, 2013, Nature Geoscience, 6, 661. doi:10.1038/ngeo1892

[64] Ramirez, R. M. & Kaltenegger, L. The Habitable Zones of Pre-main-sequence Stars, 2014, ApJ, 797, L25. doi:10.1088/2041-8205/797/2/L25

[65] Chaverot, G., Bolmont, E., & Turbet, M. First exploration of the runaway greenhouse transition with a GCM, 2023, A&A, 680, A103. doi:10.1051/0004-6361/202346936

[66] Ramirez, R. M. & Kaltenegger, L. A Volcanic Hydrogen Habitable Zone, 2017, ApJ, 837, L4.

[67] Meadows, V. S. & Barnes, R. K. 2018, Handbook of Exoplanets, 57.

[68] Ruderman, M. A. Possible Consequences of Nearby Supernova Explosions for Atmospheric Ozone and Terrestrial Life, 1974, Science, 184, 1079

[69] Thorsett, S. E. Terrestrial Implications of Cosmological Gamma-Ray Burst Models, 1995, ApJ, 444, L53

[70] Gehrels, N., Chincarini, G., Giommi, P., et al. The Swift Gamma-Ray Burst Mission, 2004, ApJ, 611, 1005

[71] Melott, A. L. & Thomas, B. C. Astrophysical Ionizing Radiation and Earth: A Brief Review and Census of Intermittent Intense Sources, 2011, Astrobiology, 11, 343

[72] Piran, T. & Jimenez, R. Possible Role of Gamma Ray Bursts on Life Extinction in the Universe, 2014, Phys Rev Lett, 113, 231102

[73] Spinelli, R., Ghirlanda, G., Haardt, F., et al. The best place and time to live in the Milky Way, 2021, A&A, 647, A41. %doi:10.1051/0004-6361/202039507

[74] Spinelli, R. & Ghirlanda, G. The Impact of GRBs on Exoplanetary Habitability, 2023, Universe, 9, 60. %doi:10.3390/universe9020060

[75] Sanz-Forcada, J., Ribas, I., Micela, G., et al. A scenario of planet erosion by coronal radiation, 2010, A&A, 511, L8

[76] Maggio, A., Pillitteri, I., Argiroffi, C., et al. X-Ray and Ultraviolet Emission of the Young Planet-hosting Star V1298 Tau from Coordinated Observations with XMM-Newton and Hubble Space Telescope, 2023, ApJ, 951, 18. %doi:10.3847/1538-4357/acd339

PoS(FRAPWS2024)062

[77] Sagan, C., Ultraviolet selection pressure on the earliest organisms, 1973, Journal of theoretical biology, 39, 195

[78] Buccino, A. P., Lemarchand, G. A., & Mauas, P. J. D. UV habitable zones around M stars, 2007, Icarus, 192, 582

[79] Toupance, G., Bossard, A., & Raulin, F. 1977, Far UV irradiation of model prebiotic atmospheres, Origins of Life, 8, 259.

[80] Powner, M. W., Gerland, B., & Sutherland, J. D. Synthesis of activated pyrimidine ribonucleotides in prebiotically plausible conditions, 2009, Nature, 459, 239.

[81] Ritson, D. & Sutherland, J. D. Prebiotic synthesis of simple sugars by photoredox systems chemistry, 2012, Nature Chemistry, 4, 895.

[82] Patel, B. H., Percivalle, C., Ritson, D. J., et al. Common origins of RNA, protein and lipid precursors in a cyanosulfidic protometabolism, 2015, Nature Chemistry, 7, 301.

[83] Xu, J., Ritson, D. J., Ranjan,S., Todd, Z. R., Sasselov, D. D., Sutherland, J. D., Photochemical reductive homologation of hydrogen cyanide using sulfite and ferrocyanide, 2018, Chem. Commun., 54, 44

[84] Rimmer, Paul B. and Xu, Jianfeng and Thompson, Samantha J. and Gillen, Ed and Sutherland, John D. and Queloz, Didier, The origin of RNA precursors on exoplanets, 2018, American Association for the Advancement of Science

[85] Spinelli, R., Borsa, F., Ghirlanda, G., et al. 2019, A&A, The high-energy radiation environment of the habitable-zone super-Earth LHS 1140b, 627, A144. doi:10.1051/0004-6361/201935636

[86] Spinelli, R., Borsa, F., Ghirlanda, G., et al. 2023, MNRAS, The ultraviolet habitable zone of exoplanets, 522, 1, 1411. doi:10.1093/mnras/stad928

[87] Roming, P. W. A., Kennedy, T. E., Mason, K. O., et al. The Swift Ultra-Violet/Optical Telescope, 2005, Space Sci Rev, 120, 95.

[88] Spinelli, R., Borsa, F., Ghirlanda, G., et al. 2024, MNRAS, The time evolution of the ultraviolet habitable zone, 533, 1, L76. doi:10.1093/mnrasl/slae064

[89] Richey-Yowell, T., Shkolnik, E. L., Schneider, A. C., et al. HAZMAT. IX. An Analysis of the UV and X-Ray Evolution of Low-mass Stars in the Era of Gaia, 2023, ApJ, 951, 44.

[90] Dotter, A. MESA Isochrones and Stellar Tracks (MIST) 0: Methods for the Construction of Stellar Isochrones, 2016, ApJS, 222, 8.

[91] Choi, J., Dotter, A., Conroy, C., et al. Mesa Isochrones and Stellar Tracks (MIST). I. Solar-scaled Models, 2016, ApJ, 823, 102.

[92] Burn, R., Schlecker, M., Mordasini, C., et al. The New Generation Planetary Population Synthesis (NGPPS). IV. Planetary systems around low-mass stars, 2021, A&A, 656, A72. doi:10.1051/0004-6361/202140390

[93] Günther, M. N., Zhan, Z., Seager, S., et al. Stellar Flares from the First TESS Data Release: Exploring a New Sample of M Dwarfs, 2020, AJ, 159, 60.

[94] Kumar, P. & Zhang, B. The Physics of Gamma-Ray Bursts and Relativistic Jets, 2015, Phys Rep, 561, 1. doi:10.1016/j.physrep.2014.09.008

[95] Thomas, B. C., Jackman, C. H., Melott, A. L., et al. Terrestrial Ozone Depletion due to a Milky Way Gamma-Ray Burst, 2005, ApJ, 622, L153

[96] Melott, A. L., Lieberman, B. S., Laird, C. M., et al. Did a gamma-ray burst initiate the late Ordovician mass extinction?, 2004, International Journal of Astrobiology, 3, 55. doi:10.1017/S1473550404001910

[97] Lineweaver, C. H., Fenner, Y., & Gibson, B. K. The Galactic Habitable Zone and the Age Distribution of Complex Life in the Milky Way, 2004, Science, 303, 59

[98] Gowanlock, M. G. & Morrison, I. S. The Habitability of our Evolving Galaxy, 2018, arXiv:1802.07036

[99] Prantzos, N. On the "Galactic Habitable Zone", 2008, Space Sci Rev, 135, 313. doi:10.1007/s11214-007-9236-9

[100] Spitoni, E., Matteucci, F., & Sozzetti, A. The galactic habitable zone of the Milky Way and M31 from chemical evolution models with gas radial flows, 2014, MNRAS, 440, 2588

[101] Spitoni, E., Gioannini, L., & Matteucci, F. Galactic habitable zone around M and FGK stars with chemical evolution models that include dust, 2017, A&A, 605, A38. doi:10.1051/0004-6361/201730545

[102] Gowanlock, M. G., Patton, D. R., & McConnell, S. M. A model of habitability within the Milky Way galaxy, 2011, Astrobiology, 11,

[103] Morrison, I. S. & Gowanlock, M. G. Extending Galactic Habitable Zone Modeling to Include the Emergence of Intelligent Life, 2015, Astrobiology, 15, 683. doi:10.1089/ast.2014.1192

[104] Forgan, D., Dayal, P., Cockell, C., et al. Evaluating galactic habitability using high-resolution cosmological simulations of galaxy formation , 2017, International Journal of Astrobiology, 16, 60. doi:10.1017/S1473550415000518

[105] Vukotić, B., Steinhauser, D., Martinez-Aviles, G., et al. 'Grandeur in this view of life': N-body simulation models of the Galactic habitable zone, 2016, MNRAS, 459, 3512

[106] Woosley, S. E., Langer, N., & Weaver, T. A. The Evolution of Massive Stars Including Mass Loss: Presupernova Models and Explosion, 1993, ApJ, 411, 823

[107] Heger, A., Fryer, C. L., Woosley, S. E., et al. How Massive Single Stars End Their Life, 2003, ApJ, 591, 288

[108] Woosley, S. E. & Heger, A. The Progenitor Stars of Gamma-Ray Bursts, 2006, ApJ, 637, 914

[109] MacFadyen, A. I. & Woosley, S. E. Collapsars: Gamma-Ray Bursts and Explosions in "Failed Supernovae", 1999, ApJ, 524, 262. doi:10.1086/307790

[110] Yoon, S.-C., Langer, N., & Norman, C. Single star progenitors of long gamma-ray bursts. I. Model grids and redshift dependent GRB rate, 2006, A&A, 460, 199

[111] Vergani, S. D., Salvaterra, R., Japelj, J., et al. Are long gamma-ray bursts biased tracers of star formation? Clues from the host galaxies of the Swift/BAT6 complete sample of LGRBs . I. Stellar mass at z < 1, 2015, A&A, 581, A102. doi:10.1051/0004-6361/201425013

[112] Perley, D. A., Tanvir, N. R., Hjorth, J., et al. THE SWIFT GRB HOST GALAXY LEGACY SURVEY. II. REST-FRAME NEAR-IR LUMINOSITY DISTRIBUTION AND EVIDENCE FOR A NEAR-SOLAR METALLICITY THRESHOLD, 2016, ApJ, 817, 8. doi:10.3847/0004-637X/817/1/8

[113] Palmerio, J. T., Vergani, S. D., Salvaterra, R., et al. Are long gamma-ray bursts biased tracers of star formation? Clues from the host galaxies of the Swift/BAT6 complete sample of bright LGRBs III. Stellar masses, star formation rates, and metallicities at z > 1, 2019, A&A, 623, A26

[114] Ghirlanda, G. & Salvaterra, R. The Cosmic History of Long Gamma Ray Bursts. *ArXiv E-prints*. pp. earXiv:2206.06390 (2022,6)

[115] Naab, T. & Ostriker, J. P. A simple model for the evolution of disc galaxies: the Milky Way, 2006, MNRAS, 366, 899

[116] Naab, T. & Ostriker, J. P. Are disk galaxies the progenitors of giant ellipticals?, 2009, ApJ, 690, 1452